Available online at www.sciencedirect.com
ScienceDirect
Journal of Sound and Vibration 308 (2007) 212–230
JOURNAL OF SOUND AND VIBRATION
www.elsevier.com/locate/jsvi

Effects of delayed feedback control on nonlinear vibration absorber system

Yan-Ying Zhao, Jian Xu*

School of Aerospace Engineering and Applied Mechanics, Tongji University, Shanghai 200092, PR China

Received 12 November 2006; received in revised form 23 April 2007; accepted 22 July 2007
Available online 31 August 2007

Abstract

The delayed feedback control is applied to suppress the vibration of vertical displacement in a two-degree-of-freedom nonlinear system with external excitation. Effects of both positive and negative feedback control are observed when the primary resonance and 1:1 internal resonance occur in the system simultaneously. The method of multiple scales is employed to obtain analytical solutions of the system under consideration. With the time delay varying for a fixed gain, it is seen that the vibration can be suppressed at some values of the delay. These values form a called ''vibration suppression region'', where one can easily observe the ''maximum vibration suppression point''. At this point, the vertical vibration could be suppressed about 65% for the positive feedback and 86% for the negative one by comparing with the nonlinear vibration absorber without delayed feedback control. However, the vibration suppression is invalid at some values of the delay. Effects of the gain on the vibration suppression are also investigated. The dynamical behaviors became complex with the gain increasing at some values of the delay, but the vibration can be suppressed more efficiently at other values. It implies that one can always choose a suitable delay and gain to achieve a vibration suppression. All analytical predictions of this paper are in good agreement with the numerical simulation.

1. Introduction

The theory and technique of vibration suppression are extensively studied for many years. There are three fundamentally different primary methods of vibration suppression, i.e. damp shock absorber, nonlinear vibration absorber and delayed feedback control vibration absorber.

The damp shock absorber is a classical technique. It is well known that the theory and experiment about the technique of damp shock absorber are sufficiently studied in the past years. The technique of damp shock absorber is widely used in the fields of aerospace engineering, automobile industry, instrumental apparatus, weapons, architecture industry and engineering machine. In numerous damp shock absorbers, dynamic vibration absorber is the focus of attention. It is often used to remove undesirable oscillations from the primary system. For example, mass–spring–dashpot dynamical vibration absorber is installed in a helicopter cockpit [1].

*Corresponding author. Tel.: +86 21 65985364; fax: +86 21 55041398.
E-mail address: xujian@mail.tongji.edu.cn (J. Xu).

0022-460X/$ - see front matter © 2007 Elsevier Ltd. All rights reserved.
doi:10.1016/j.jsv.2007.07.041

Recently, nonlinear vibration absorber is designed based on nonlinear dynamics. The effectiveness of the nonlinear vibration absorber was first outlined by Roberson [2]. Arnold [3] concluded that a softening spring would increase the vibration suppression bandwidth, while the hardening spring would do contrarily. Lee and Shaw [4] investigated the dynamics of a pair of identical centrifugal pendulum vibration absorbers. They indicated that the absorbers could reduce torsional vibrations in rotating machines for effects of nonlinear behavior of the absorbers. From a physical point of view, nonlinearity of the spring could increase the suppression bandwidth of the absorbers for some cases. The saturation phenomenon was first discovered by Nayfeh et al. [5] for motions of ships. The saturation phenomenon, that is, the response amplitude of the primary system, linearly increases with the amplitude of excitation. However, once the amplitude of the excitation passes a critical value, the response amplitude of the primary system is saturated at a specific value and all the additional energy from the excitation is channeled to the secondary system. For the passive vibration absorber system, it is too complex to design, and the ratio of internal resonance is difficult to control exactly. Thus, many authors considered active vibration control, such as analog electric-circuit controller [6], digital signal [7], piezoelectric patches [8] and Terfenol-D [9], to suppress vibrations.

The technique of delayed feedback control vibration absorber is a new technique of vibration suppression. In fact, time delay in control system is derived from measurements of system states, by physical properties of the equipment used for control and transport delay, by performing on-line computation, filtering and processing data and by calculating and executing the control forces as required. Therefore, the studies of control system with time delay have been developed in various research fields, such as mechanics [10], mechanical engineering [11–13], combustion dynamics [14], aerospace engineering [15], communication [16] and medicine [17,18]. The delayed feedback control has been frequently applied in controlling chaos, improving stability of periodic solutions and stabilizing unstable equilibria since the pioneering work was given by Pyragas [19]. Our previous research [20] also showed that the delay may be used as a simple but efficient "switch" to control motions of a system: either from order motion to chaos or from chaotic motion to order for different applications. Delayed position feedback control to dynamical structures was first presented by Olgac and Holm-Hansen [21] by introducing a delayed resonator. The technique offers a number of attractive advantages in eliminating tonal vibrations of the primary system, such as real time tunability, wide range of frequency, perfect tonal suppression and simplicity of the control. Then, many results were obtained for linear systems [22–25].

It should be noted that the present absorber with delayed resonator is only considered for the case that the system is linear. It follows from the above review that the delayed position feedback control and nonlinear vibration absorber have their advantages, respectively. Motivated by these advantages, we will here design a device together with delayed feedback control and nonlinear vibration absorber and investigate effects of the device on vibration suppression in a two-degree-of-freedom system. To the best knowledge of the authors, the delayed feedback control is not applied for the system with nonlinear vibration absorber.

The present paper is organized as follows. The formulation of the problem is shown in Section 2. In Sections 3 and 4, the perturbation analysis and the stability of the equilibrium solutions are given. The analytical solutions and numerical simulations for the positive and negative delayed feedback control are presented in Sections 5 and 6, respectively. Concluding remarks are presented in Section 7.

2. Formulation of the problem

A two-degree-of-freedom model of a nonlinear vibration absorber is described in Ariaratnam [26], Malhotra and Srinamachchivaya [27] and Zhang and Li [28]. In this paper, a position feedback with time delay is introduced into the above model to control the vibrations of the vertical displacement in the dynamical system, as shown in Fig. 1.

The system consists of a grid body of mass m and the relevant moment inertia I, and is supported by two identically placed spring–dashpot systems. The dashpot systems are assumed to be linear with viscous damping coefficient β, and the springs are assumed to be nonlinear with force–displacement ($f-\delta$) relationship given as $f = k\delta + c\delta^3$. Assuming the support is given a periodic excitation ($F(t) = A\cos\omega t$), and let d denote the distance from the vertical axis of symmetry to the point of attachment of either of spring–dashpot units, q_1 and q_2 denote the relative vertical displacement and pitching angle. A time delayed position feedback

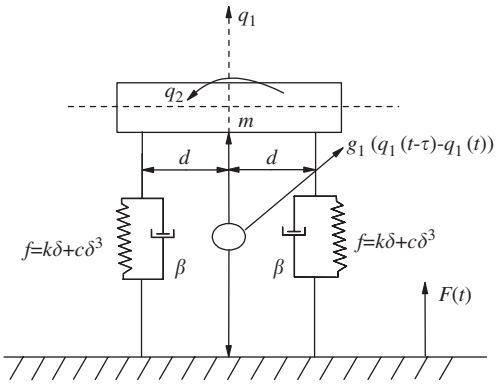

Fig. 1. A model describing the nonlinear vibration absorber with delayed feedback.

$g_1\big(q_1(t-\tau)-q_1(t)\big)$ is introduced to the nonlinear dynamical system. Then the governing equations of motions describing the vertical displacement q_1 and the pitching angle q_2 can be expressed as

$$m\ddot{q}_1 + 2\beta\dot{q}_1 + 2kq_1 + 2c(q_1^3 + 3d^2q_1q_2^2) + g_1(q_{1\tau} - q_1) + m\ddot{F} = 0, \tag{1}$$

$$I\ddot{q}_2 + 2d^2\beta\dot{q}_2 + 2d^2kq_2 + 2cd^2(d^2q_2^3 + 3q_1^2q_2) = 0, \tag{2}$$

where $q_{1\tau} = q_1(t-\tau)$. It should be noted that the delayed feedback disappears in Eqs. (1) and (2) when $\tau = 0$ and Eqs. (1) and (2) are identical to those in Refs. [26–28]. Thus, it is easy to observe effects of the delayed feedback when $\tau \neq 0$.

3. Perturbation analysis

Firstly, a set of dimensionless (or normalized) variables are defined as

$$t^* = \frac{\Omega}{\omega}t, \quad x_1 = \frac{q_1}{d}, \quad x_2 = q_2, \quad \varepsilon\mu_1 = \frac{2\beta\Omega}{m\omega}, \quad \varepsilon\mu_2 = \frac{2d^2\beta\Omega}{I\omega}, \quad \omega_1^2 = \frac{2k\Omega^2}{m\omega^2}, \quad \omega_2^2 = \frac{2d^2k\Omega^2}{I\omega^2},$$
$$\varepsilon\alpha_1 = \frac{2cd^2\Omega^2}{m\omega^2}, \quad \varepsilon\alpha_2 = \frac{6cd^2\Omega^2}{m\omega^2}, \quad \varepsilon\beta_1 = \frac{2d^4c\Omega^2}{I\omega^2}, \quad \varepsilon\beta_2 = \frac{6cd^4\Omega^2}{I\omega^2}, \quad \varepsilon f = \frac{A\Omega^2}{d},$$
$$\varepsilon g = \frac{g_1 d\Omega^2}{m\omega^2}, \quad \tau^* = \frac{\Omega}{\omega}\tau.$$

It follows from Ref. [28], both damping β and nonlinear stiffness c are weak or very small, which implies ε can be considered as a perturbation parameter with $0 < \varepsilon \ll 1$. Dropping the asterisk for convenience, one can write Eqs. (1) and (2) as

$$\ddot{x}_1 + \omega_1^2 x_1 = \varepsilon(f\cos\Omega t - \mu_1\dot{x}_1 - \alpha_1 x_1^3 - \alpha_2 x_1 x_2^2 - g x_{1\tau} + g x_1), \tag{3}$$

$$\ddot{x}_2 + \omega_2^2 x_2 = \varepsilon(-\mu_2\dot{x}_2 - \beta_1 x_2^3 - \beta_2 x_1^2 x_2), \tag{4}$$

where Ω is a dimensionless frequency, and $x_{1\tau} = x_1(t-\tau)$.

It is assumed that d equals the radius ρ of gyration for the relevant moment inertia I, that is, $I = m\rho^2 = md^2$. It yields that $\alpha_1 = \beta_1$ and $\alpha_2 = \beta_2$.

The method of multiple scales [29] is employed to seek second-order approximate solutions of Eqs. (3) and (4) in the following form:

$$x_1(t,\varepsilon) = x_{10}(T_0, T_1) + \varepsilon x_{11}(T_0, T_1) + \ldots, \tag{5}$$

$$x_2(t,\varepsilon) = x_{20}(T_0, T_1) + \varepsilon x_{21}(T_0, T_1) + \ldots, \tag{6}$$

$$x_{1\tau}(t,\varepsilon) = x_{10\tau}(T_0,T_1) + \varepsilon x_{11\tau}(T_0,T_1) + \ldots, \tag{7}$$

where $T_0 = t$ is the fast time scale and $T_1 = \varepsilon t$ is a slow time scale envelope of the response. The derivatives with respect to time are expressed in term of the new scales as

$$\frac{\mathrm{d}}{\mathrm{d}t} = D_0 + \varepsilon D_1 + \ldots, \tag{8}$$

$$\frac{\mathrm{d}^2}{\mathrm{d}t^2} = D_0^2 + 2\varepsilon D_0 D_1 + \ldots, \tag{9}$$

where $D_k = \partial/\partial T_k$, $k = 0, 1$.

Substituting Eqs. (5)–(9) into Eqs. (3) and (4) and equating coefficients of like powers of ε yields

Order ε^0:

$$D_0^2 x_{10} + \omega_1^2 x_{10} = 0, \tag{10}$$

$$D_0^2 x_{20} + \omega_2^2 x_{20} = 0. \tag{11}$$

Order ε^1:

$$D_0^2 x_{11} + \omega_1^2 x_{11} = f\cos\Omega T_0 - 2D_0D_1x_{10} - \mu_1 D_0 x_{10} - \alpha_1 x_{10}^3 - \alpha_2 x_{10}x_{20}^2 - g x_{10\tau} + g x_{10}, \tag{12}$$

$$D_0^2 x_{21} + \omega_2^2 x_{21} = -2D_0D_1x_{20} - \mu_2 D_0 x_{20} - \beta_1 x_{20}^3 - \beta_2 x_{10}^2 x_{20}. \tag{13}$$

The solutions of Eqs. (10) and (11) can be expressed as

$$x_{10} = A_1(T_1)\mathrm{e}^{\mathrm{i}\omega_1 T_0} + \mathrm{cc}, \tag{14}$$

$$x_{20} = A_2(T_1)\mathrm{e}^{\mathrm{i}\omega_2 T_0} + \mathrm{cc}, \tag{15}$$

where A_1 and A_2 are arbitrary functions at this level of approximation, $\mathrm{i} \equiv \sqrt{-1}$, and cc denotes complex conjugate. The external excitation and the delayed feedback are expressed in complex forms given by

$$f\cos\Omega T_0 = \frac{1}{2} f \mathrm{e}^{\mathrm{i}\Omega T_0} + \mathrm{cc} \tag{16}$$

and

$$x_{10\tau} = A_{1\tau}(T_1)\mathrm{e}^{\mathrm{i}\omega_1(T_0-\tau)} + \mathrm{cc}. \tag{17}$$

Expand $A_{1\tau}$ in a Taylor series [30] under the assumption that the product of time delay and the small parameter ε is small compared to unity:

$$A_{1\tau} = A_1(T_1 - \varepsilon\tau) = A_1(T_1) - \varepsilon\tau A_1'(T_1) + \varepsilon^2\tau^2 A_1'' + \ldots. \tag{18}$$

Substituting Eqs. (14)–(18) into Eqs. (12) and (13) yields

$$\begin{aligned} D_0^2 x_{11} + \omega_1^2 x_{11} = {} & \frac{1}{2} f \mathrm{e}^{\mathrm{i}\Omega T_0} - \mathrm{i}\omega_1(2A_1' + \mu_1 A_1)\mathrm{e}^{\mathrm{i}\omega_1 T_0} - \alpha_1(A_1^3\mathrm{e}^{\mathrm{i}3\omega_1 T_0} + 3A_1^2\bar{A}_1\mathrm{e}^{\mathrm{i}\omega_1 T_0}) \\ & - \alpha_2\left(A_1A_2^2\mathrm{e}^{\mathrm{i}(\omega_1+2\omega_2)T_0} + \bar{A}_1A_2^2\mathrm{e}^{\mathrm{i}(-\omega_1+2\omega_2)T_0} + 2A_1A_2\bar{A}_2\mathrm{e}^{\mathrm{i}\omega_1 T_0}\right) \\ & - gA_1\mathrm{e}^{\mathrm{i}\omega_1(T_0-\tau)} + gA_1\mathrm{e}^{\mathrm{i}\omega_1 T_0} + \mathrm{cc}, \end{aligned} \tag{19}$$

$$\begin{aligned} D_0^2 x_{21} + \omega_2^2 x_{21} = {} & -\mathrm{i}\omega_2(2A_2' + \mu_2 A_2)\mathrm{e}^{\mathrm{i}\omega_2 T_0} - \beta_1(A_2^3\mathrm{e}^{\mathrm{i}3\omega_2 T_0} + 3A_2^2\bar{A}_2\mathrm{e}^{\mathrm{i}\omega_2 T_0}) \\ & - \beta_2\left(A_2A_1^2\mathrm{e}^{\mathrm{i}(\omega_2+2\omega_1)T_0} + \bar{A}_2A_1^2\mathrm{e}^{\mathrm{i}(-\omega_2+2\omega_1)T_0} + 2A_1A_2\bar{A}_1\mathrm{e}^{\mathrm{i}\omega_2 T_0}\right) + \mathrm{cc}, \end{aligned} \tag{20}$$

where $()' \equiv \partial()/\partial T_1 = \partial()/\partial(\varepsilon t)$. In the following part, a case of the primary resonance and 1:1 internal resonance is considered. The nearness of the external resonance is represented by a detuning parameter σ_1 defined by

$$\Omega = \omega_1 + \varepsilon\sigma_1. \tag{21}$$

To describe the nearness of the internal resonance, a detuning parameter σ_2 is introduced and defined by

$$\omega_1 = \omega_2 - \varepsilon\sigma_2. \tag{22}$$

Substituting Eqs. (21) and (22) into Eqs. (19)–(20) and setting the coefficients of the secular terms to zero yielding the solvability conditions given by

$$\frac{1}{2}f\mathrm{e}^{\mathrm{i}\sigma_1 T_1} - \mathrm{i}\omega_1(2A_1' + \mu_1 A_1) - 3\alpha_1 A_1^2\bar{A}_1 - \alpha_2(\bar{A}_1 A_2^2\mathrm{e}^{\mathrm{i}2\sigma_2 T_1} + 2A_1A_2\bar{A}_2) - gA_1\mathrm{e}^{-\mathrm{i}\omega_1\tau} + gA_1 = 0, \tag{23}$$

$$-\mathrm{i}\omega_2(2A_2' + \mu_2 A_2) - 3\beta_1 A_2^2\bar{A} - \beta_2(\bar{A}_2 A_1^2\mathrm{e}^{-\mathrm{i}2\sigma_2 T_1} + 2A_1A_2\bar{A}_1) = 0. \tag{24}$$

Introducing polar notation $A_1(T_1) = \frac{1}{2}a_1(T_1)\mathrm{e}^{\mathrm{i}\theta_1(T_1)}$ and $A_2(T_1) = \frac{1}{2}a_2(T_1)\mathrm{e}^{\mathrm{i}\theta_2(T_1)}$ into Eqs. (23)–(24) and setting the coefficients of the real and imaginary parts to zero yields the algebraic equations given by

$$a_1' = \frac{1}{\omega_1}\left[\frac{1}{2}f\,\sin\,\phi_1 - \frac{1}{2}\omega_1\mu_1 a_1 + \frac{1}{8}\alpha_2 a_1 a_2^2\,\sin(2\phi_2) + \frac{1}{2}ga_1\,\sin(\omega_1\tau)\right], \tag{25}$$

$$a_2' = \frac{1}{\omega_2}\left[-\frac{1}{2}\omega_2\mu_2 a_2 - \frac{1}{8}\beta_2 a_1^2 a_2\,\sin(2\phi_2)\right], \tag{26}$$

$$\begin{aligned}\phi_1' a_1 = \frac{1}{\omega_1}\Bigg[&\frac{1}{2}f\,\cos\,\phi_1 + \omega_1\sigma_1 a_1 - \frac{3}{8}\alpha_1 a_1^3 - \frac{1}{4}\alpha_2 a_1 a_2^2 - \frac{1}{8}\alpha_2 a_1 a_2^2\,\cos(2\phi_2)\\ &-\frac{1}{2}ga_1\,\cos(\omega_1\tau) + \frac{1}{2}ga_1\Bigg],\end{aligned} \tag{27}$$

$$(\phi_1' + \phi_2')a_2 = \frac{1}{\omega_2}\left[\omega_2(\sigma_1 - \sigma_2)a_2 - \frac{3}{8}\beta_1 a_2^3 - \frac{1}{4}\beta_2 a_1^2 a_2 - \frac{1}{8}\beta_2 a_1^2 a_2\,\cos(2\phi_2)\right], \tag{28}$$

where $\phi_1 = \sigma_1 T_1 - \theta_1$, $\phi_2 = \theta_1 - \theta_2 - \sigma_2 T_1$.

4. Equilibrium solutions and their stability

It is well known that the approximate solutions of Eqs. (3)–(4) correspond to the equilibrium solutions of Eqs. (25)–(28) by setting $a_1' = a_2' = \phi_1' = \phi_2' = 0$, which implies that one has to solve four transcendental equations. However, it is difficult even by numerical methods. To avoid such difficulty, we transform Eqs. (25)–(28) into the form of the Cartesian coordinates given by

$$\begin{aligned}p_1' = \frac{1}{\omega_1}\Bigg\{&-\frac{1}{2}\omega_1\mu_1 p_1 - \omega_1\sigma_1 q_1 + \frac{3}{8}\alpha_1 q_1(p_1^2 + q_1^2) + \frac{1}{4}\alpha_2 q_1(p_2^2 + q_2^2)\\ &+\frac{1}{2}g\left[\sin(\omega_1\tau)p_1 + \cos(\omega_1\tau)q_1 - q_1\right] + \frac{1}{8}\alpha_2\left[2p_1p_2q_2 + q_1(q_2^2 - p_2^2)\right]\Bigg\},\end{aligned} \tag{29}$$

$$\begin{aligned}q_1' = \frac{1}{\omega_1}\Bigg\{&\frac{1}{2}f - \frac{1}{2}\omega_1\mu_1 q_1 + \omega_1\sigma_1 p_1 - \frac{3}{8}\alpha_1 p_1(p_1^2 + q_1^2) - \frac{1}{4}\alpha_2 p_1(p_2^2 + q_2^2)\\ &+\frac{1}{2}g\left[\sin(\omega_1\tau)q_1 - \cos(\omega_1\tau)p_1 + p_1\right] - \frac{1}{8}\alpha_2\left[2q_1p_2q_2 + p_1(p_2^2 - q_2^2)\right]\Bigg\},\end{aligned} \tag{30}$$

$$\begin{aligned}p_2' = \frac{1}{\omega_2}\Bigg\{&-\frac{1}{2}\omega_2\mu_2 p_2 - \omega_2(\sigma_1 - \sigma_2)q_2 + \frac{3}{8}\beta_1 q_2(p_2^2 + q_2^2) + \frac{1}{4}\beta_2 q_2(p_1^2 + q_1^2)\\ &+\frac{1}{8}\beta_2\left[2p_2p_1q_1 + q_2(q_1^2 - p_1^2)\right]\Bigg\},\end{aligned} \tag{31}$$

$$q_2' = \frac{1}{\omega_2}\left\{-\frac{1}{2}\omega_2\mu_2 q_2 + \omega_2(\sigma_1-\sigma_2)p_2 - \frac{3}{8}\beta_1 p_2(p_2^2+q_2^2) - \frac{1}{4}\beta_2 p_2(p_1^2+q_1^2) - \frac{1}{8}\beta_2\left[2q_2p_1q_1 + p_2(p_1^2-q_1^2)\right]\right\}, \tag{32}$$

where $p_1 = a_1\cos\phi_1$, $q_1 = a_1\sin\phi_1$, $p_2 = a_2\cos(\phi_1+\phi_2)$ and $q_2 = a_2\sin(\phi_1+\phi_2)$.

To determine the stability of the equilibrium solutions, Eqs. (29)–(32) are perturbed by a small perturbation. The perturbation equations are shown as follows:

$$\{\Delta p_1', \Delta q_1', \Delta p_2', \Delta q_2'\}^{\mathrm{T}} = [J]\{\Delta p_1, \Delta q_1, \Delta p_2, \Delta q_2\}^{\mathrm{T}}, \tag{33}$$

where T denotes transpose of the matrix, $[J]$ is the Jacobian matrix. Equation of the eigenvalues corresponding to a fixed equilibrium solution may be expressed as

$$\lambda^4 + \delta_1\lambda^3 + \delta_2\lambda^2 + \delta_3\lambda + \delta_4 = 0, \tag{34}$$

where λ denotes eigenvalues of matrix $[J]$, δ_1, δ_2, δ_3 and δ_4 are coefficients of the equation.

Routh–Hurwitz criterion is used to establish the stability of the equilibrium solutions. Accordingly, the necessary and sufficient condition for the stable system is

$$\delta_1 > 0, \quad \delta_1\delta_2 - \delta_3 > 0, \quad \delta_3(\delta_1\delta_2 - \delta_3) - \delta_1^2\delta_4 > 0, \quad \delta_4 > 0. \tag{35}$$

The condition for the occurrence static bifurcation may occur:

$$\delta_4 = 0. \tag{36}$$

The necessary and sufficient condition when Hopf bifurcation occurs in the system is

$$\delta_1\delta_3 > 0,\ \delta_3(\delta_1\delta_2 - \delta_3) - \delta_1^2\delta_4 = 0. \tag{37}$$

The equilibrium is stable if and only if the real parts of all eigenvalues are negative and unstable if positive, corresponding to the steady-state solutions in Eqs. (3) and (4). If a real eigenvalue changes sign, a saddle–node-type bifurcation occurs in the system, resulting in jump phenomena. If there exists a pair of complex conjugate eigenvalues and their real part changes sign, a Hopf bifurcation appears, resulting in a quasi-periodic motion in the original system.

For delayed feedback control system, it is generally grouped positive ($\varepsilon g > 0$) and negative ($\varepsilon g < 0$) feedback control according to the sign of the gain in the delayed feedback. In the following sections, the performance of the positive and negative feedback control technique with time delay is evaluated both in theoretical analysis and numerical simulation respectively. The variable parameters are taken for $\varepsilon\tau$ and εg and other parameters are fixed as $\omega_1 = 1.0$, $\omega_2 = 1.0$, $\varepsilon\alpha_1 = 0.30$, $\varepsilon\alpha_2 = 0.90$, $\varepsilon\beta_1 = 0.30$, $\varepsilon\beta_2 = 0.90$, $\varepsilon\mu_1 = 0.10$, $\varepsilon\mu_2 = 0.10$, $\varepsilon\sigma_1 = 0.10$, $\varepsilon\sigma_2 = 0$, $\varepsilon f = 0.30$.

5. Performance of the control strategy for positive delayed feedback control

Setting $p_1' = q_1' = p_2' = q_2' = 0$ in Eqs. (29)–(32) and using $a_i = \sqrt{p_i^2 + q_i^2}$ $i = 1, 2$, one may obtain the equilibrium solutions for $\varepsilon g > 0$, as shown in Fig. 2, where $\mathrm{H}_{(\cdot)}$ are denoted as the Hopf bifurcation points, $\mathrm{SN}_{(\cdot)}$ the saddle–node bifurcation points, $\mathrm{PF}_{(\cdot)}$ the pitchfork bifurcation points and $\mathrm{HD}_{(\cdot)}$ the boundary points to distinguish those unstable foci and other unstable equilibriums. The solid line represents stable solutions, dot with black represents unstable foci and dot with blank represents other unstable solutions.

Fig. 2a shows the amplitude–delay response curves when $\varepsilon g = 0.10$. The amplitude increases as $\varepsilon\tau$ increases at the beginning. Then, the amplitude decreases as $\varepsilon\tau$ increases. Furthermore, we observed that the amplitude–delay response curve is always stable at time delay space. It is inconspicuous for a tunable range of $\varepsilon\tau$ to suppress the vibration of vertical displacement. With εg increasing to 0.13, the solution undergoes a Hopf bifurcation at H_1 and H_2, as shown in Fig. 2b. It implies that the periodic solution disappears and the complicated motions may occur in the system when $\varepsilon\tau$ is located between H_1 and H_2. When εg is increased further to 0.144 and 0.145, the saddle–node bifurcation occurs at SN_1 and SN_2, yielding two stable solutions and one unstable solution coexist between SN_1 and SN_2. The solution may jump from one steady state to

another one, which depends on the initial conditions, as shown in Fig. 2c and d. A tunable range of $\varepsilon\tau$ to suppress the vibration is obtained when time delay is located between SN_1 and SN_2.

As depicted in Fig. 2e and f when $\varepsilon g = 0.155$ and 0.159, the increase of the gain yields that the unstable branch bifurcating from SN_1 or SN_2 collides with the upper stable branch such that the point at SN_1 becomes the pitchfork bifurcation one (denoted as PF_1), and a new saddle–node bifurcation point at SN_3 is obtained. In addition, two Hopf bifurcations H_3 and H_4 occurred between PF_1 and SN_2 (see Fig. 2f). There may be four

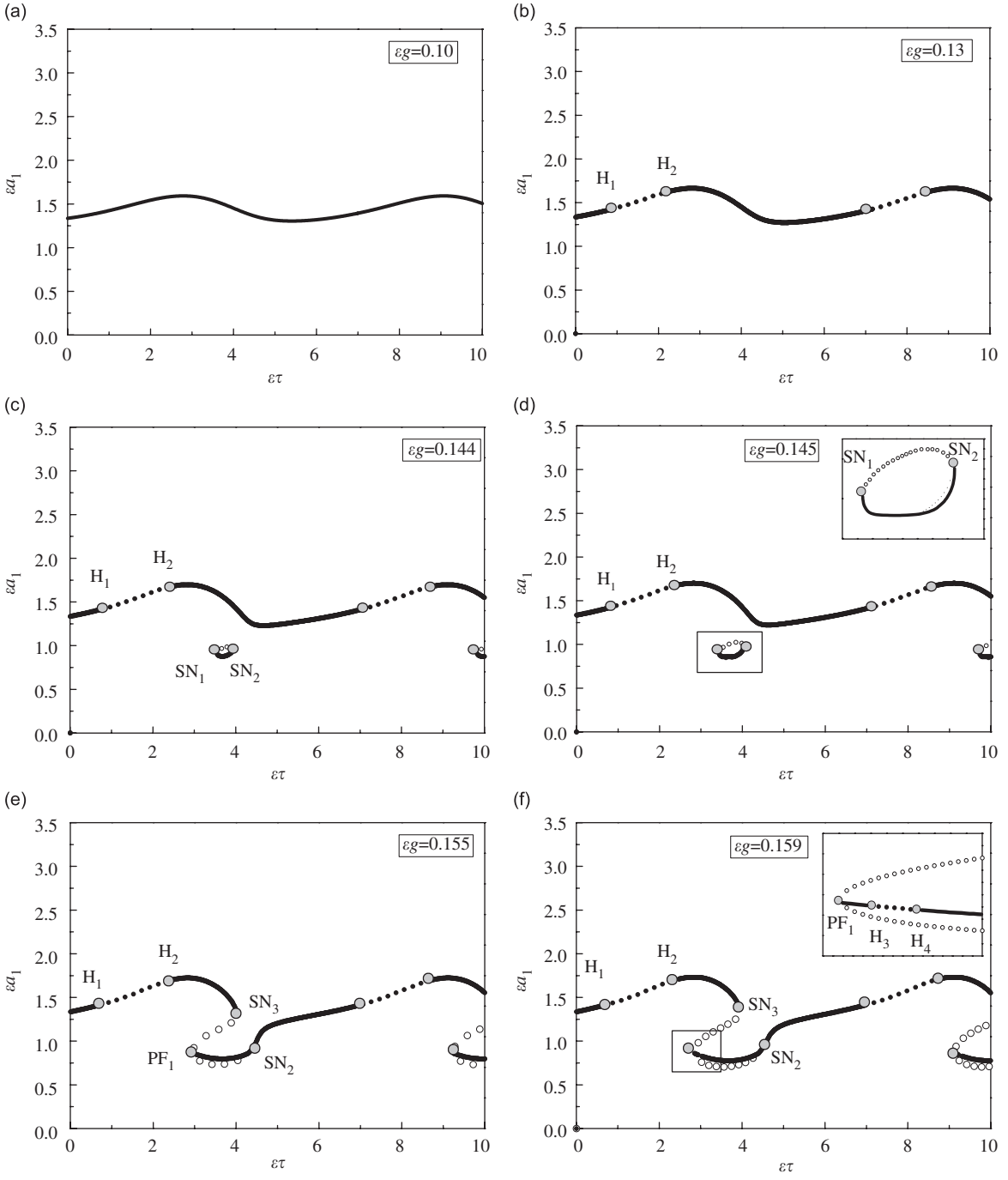

Fig. 2. Amplitude–delay response curves of vertical displacement with different gains for positive delayed feedback control.

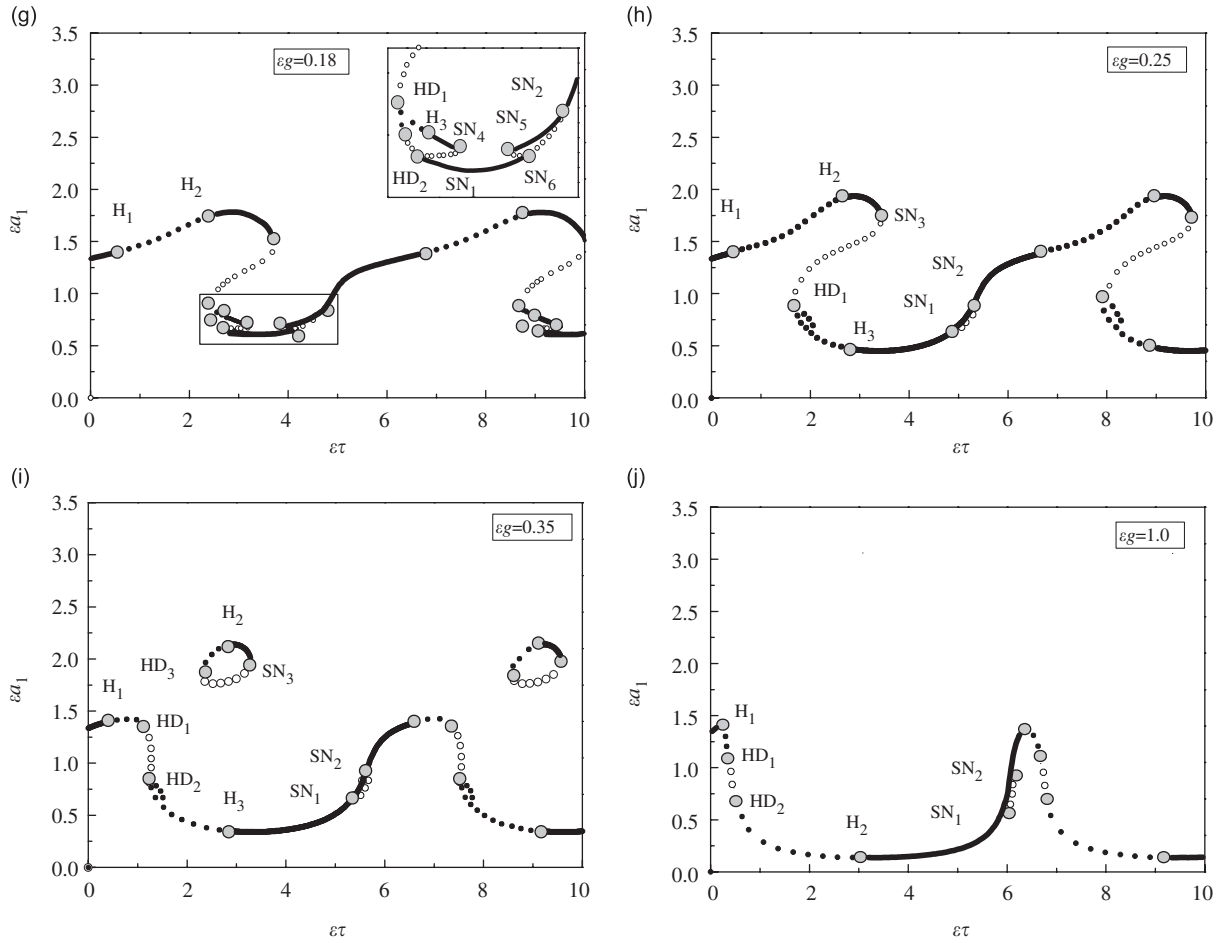

Fig. 2. (*Continued*)

solutions between PF_1 and SN_2, two stable solutions and two unstable ones. It follows from Fig. 2e and f that two possible region of vibration suppression may be obtained. One is located at the region between PF_1 and H_3, the other is between H_4 and SN_2.

The amplitude–delay response curves become complicated in Fig. 2(g), where $\varepsilon g = 0.18$. In fact, the point H_3 incorporates with PF_1 such that the points disappear and the points SN_1 and SN_6 occur again when the gain is increased gradually. Then, the upper unstable branch bifurcating from SN_1 or SN_6 collides with the stable branch from SN_2, yielding two new saddle–node bifurcation points, denoted as SN_4 and SN_5. Noting that in Fig. 2(g), there are five solutions between H_3 and SN_4, three stable solutions and two unstable ones. The system has complicated dynamical behaviors between H_3 and SN_4. It can be seen that there are several regions of vibration suppression in $\varepsilon\tau$, i.e. the region between H_3 and SN_4, the region between SN_4 and SN_5, and the region between SN_5 and SN_2. It can be seen that the region where $\varepsilon\tau$ is located in the interval [SN_4, SN_5] is the best choice, corresponding to the best performance of vibration suppression.

When the gain is changed from 0.18 to 0.25, the unstable branches bifurcating from SN_6 disappear and yield the points SN_5 that collide with SN_6 on the one hand, and the unstable branch from SN_4 shrinks such that SN_4 collides with SN_1 on the other hand. As a result, the amplitude–delay response curves become relative simple. Correspondingly, only one region of vibration suppression may be obtained between H_3 and SN_1, as shown in Fig. 2(h). A more large value of the gain yields that the topological structure of the response curve is changed (see Fig. 2i). It should be noted that the response shown in Fig. 2i is different from those in Fig. 2c

and d, where the curve from the saddle–node bifurcation is in the lower location. It implies that the attracting area corresponding to every solution is changed with the gain increasing. Thus, a tunable range of $\varepsilon\tau$ to suppress the vibration can be found much easily, as shown in Fig. 2(j).

It follows from Fig. 2 that the amplitude–delay response curves is periodic in the time delay, which suggests that it is enough to analyze the amplitude–delay response curves in one period. Fig. 2 shows also that a large value of the gain can provide more choices for $\varepsilon\tau$ to suppress the vibration. But it can lead to the system losing its stability such that the motion becomes complicated. Therefore, the gain should be modified very carefully in applications.

One has seen that the coexisted solutions, a tunable range of $\varepsilon\tau$ to suppress the vibration and complex motions may occur in the system with the gain and delay varying by the analytical method mentioned above. Now, we employ the numerical method to verify these analytical predictions based on Eqs. (3)–(4). The initial conditions are taken as $x_1(0) = x_2(0) = 10^{-4}$, $\dot{x}_1(0) = \dot{x}_2(0) = 10^{-4}$, $x_1(t) = x_2(t) = 0$, $\dot{x}_1(t) = \dot{x}_2(t) = 0$ for $t \in [-\varepsilon\tau, 0)$ in all numerical simulation except those specially given cases. The parameters are the same as those in Fig. 2.

First, the analytical results are compared with the numerical ones quantitatively. Fig. 3 shows the comparison of the results between numerical simulations and analytical solutions for amplitude–delay response curves when $\varepsilon g = 0.10$, corresponding to Fig. 2a, where the solid line represents the analytical solution and the dot with asterisk symbol the numerical result. It follows from Fig. 3 that the analytical solution is in agreement with that from the numerical simulation, which suggests that the analysis is valid.

From the above analysis, multiple solutions have been predicted with the gain and delay varying, as shown in Fig. 2(c)–(i). We take $\varepsilon g = 0.145$ and 0.18, corresponding to Fig. 2(d) and (g) respectively, to verify such analytical prediction. The numerical simulation is shown in Figs. 4 and 5. Fig. 4 shows that there are two stable solutions for two different initial conditions given by $x_1(0) = x_2(0) = \dot{x}_1(0) = \dot{x}_2(0) = 10^{-4}$and $x_1(0) = x_2(0) = \dot{x}_1(0) = \dot{x}_2(0) = 10^{-1}$ when $\varepsilon\tau = 3.40$. In Fig. 5, three different initial conditions given by $x_1(0) = x_2(0) = \dot{x}_1(0) = \dot{x}_2(0) = 10^{-4}$, $x_1(0) = x_2(0) = \dot{x}_1(0) = \dot{x}_2(0) = 10^{-2}$ and $x_1(0) = x_2(0) = \dot{x}_1(0) = \dot{x}_2(0) = 10^{-1}$ yields three coexisted stable solutions at $\varepsilon\tau = 3.0$. It follows from Figs. 4 and 5 that the analytical prediction is in agreement with the numerical simulation completely.

It has been predicted there is a tunable range of $\varepsilon\tau$ to suppress the vibration for different values of the gain. Now, we choose a case, i.e. $\varepsilon g = 0.25$, as shown in Fig. 2(h) to verify such prediction quantitatively. Fig. 6 shows the time history of the solutions corresponding to $\varepsilon\tau = 0$, $\varepsilon\tau = 3.0$ and $\varepsilon\tau = 4.0$. It is seen that the amplitude of the vertical displacement is suppressed from 1.30 to about 0.45. The oscillations of the vertical displacement are maximally suppressed amounting to about 65% for positive delayed feedback control. It should be indicated that the analytical solutions agree with numerical integration well until $\varepsilon g = 0.25$ by combining Fig. 6 with Fig. 2.

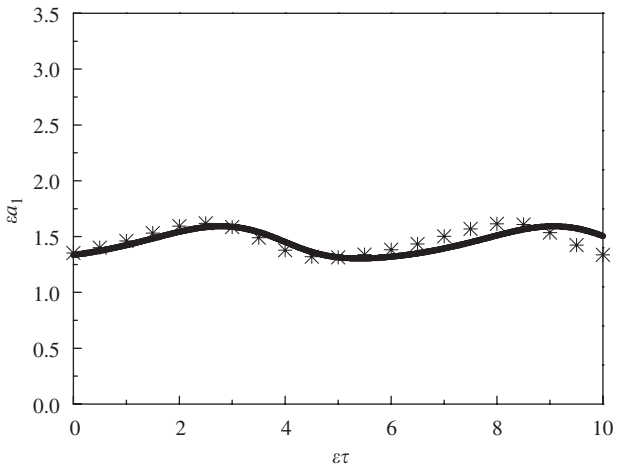

Fig. 3. Comparison between numerical simulation and analytical solution for amplitude–delay response curves when $\varepsilon g = 0.10$.

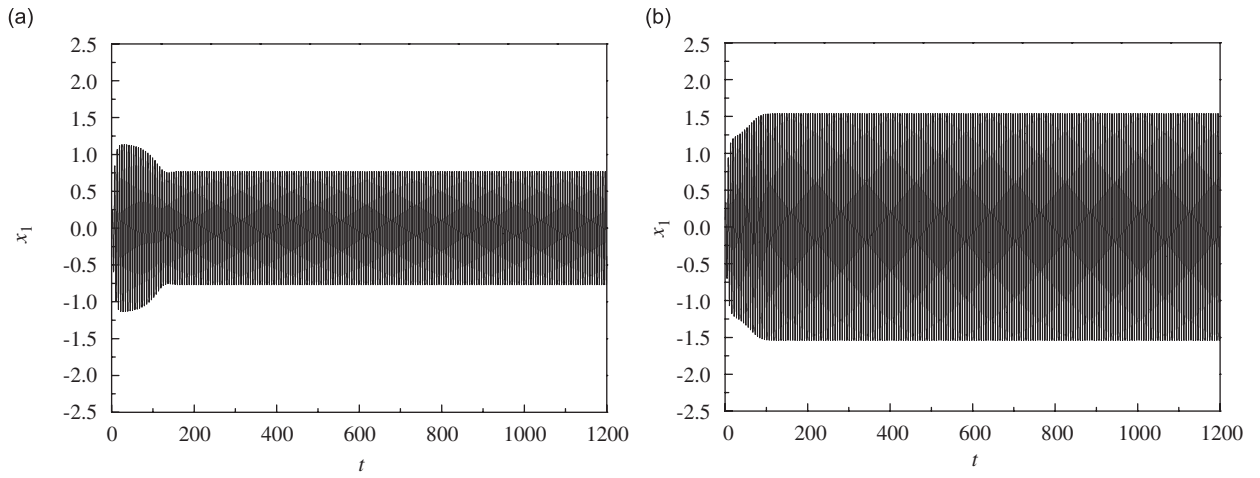

Fig. 4. Two coexisted stable solutions when $\varepsilon\tau = 3.40$ and $\varepsilon g = 0.145$ for different initial conditions given by (a) $x_1(0) = x_2(0) = \dot{x}_1(0) = \dot{x}_2(0) = 10^{-4}$and (b) $x_1(0) = x_2(0) = \dot{x}_1(0) = \dot{x}_2(0) = 10^{-1}$.

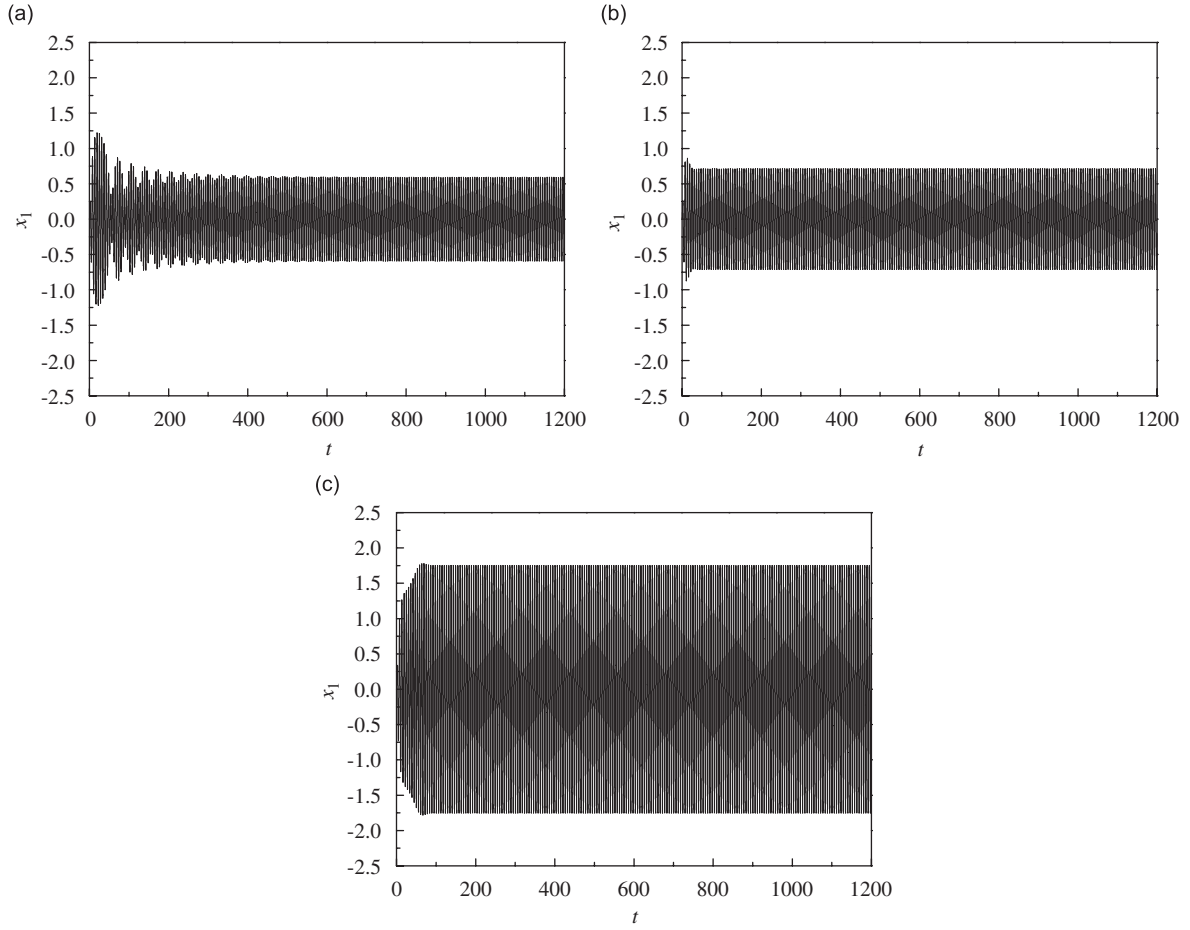

Fig. 5. Three coexisted stable solutions when $\varepsilon\tau = 3.0$ and $\varepsilon g = 0.18$ for different initial conditions given by (a) $x_1(0) = x_2(0) = \dot{x}_1(0) = \dot{x}_2(0) = 10^{-4}$, (b) $x_1(0) = x_2(0) = \dot{x}_1(0) = \dot{x}_2(0) = 10^{-2}$ and (c) $x_1(0) = x_2(0) = \dot{x}_1(0) = \dot{x}_2(0) = 10^{-1}$.

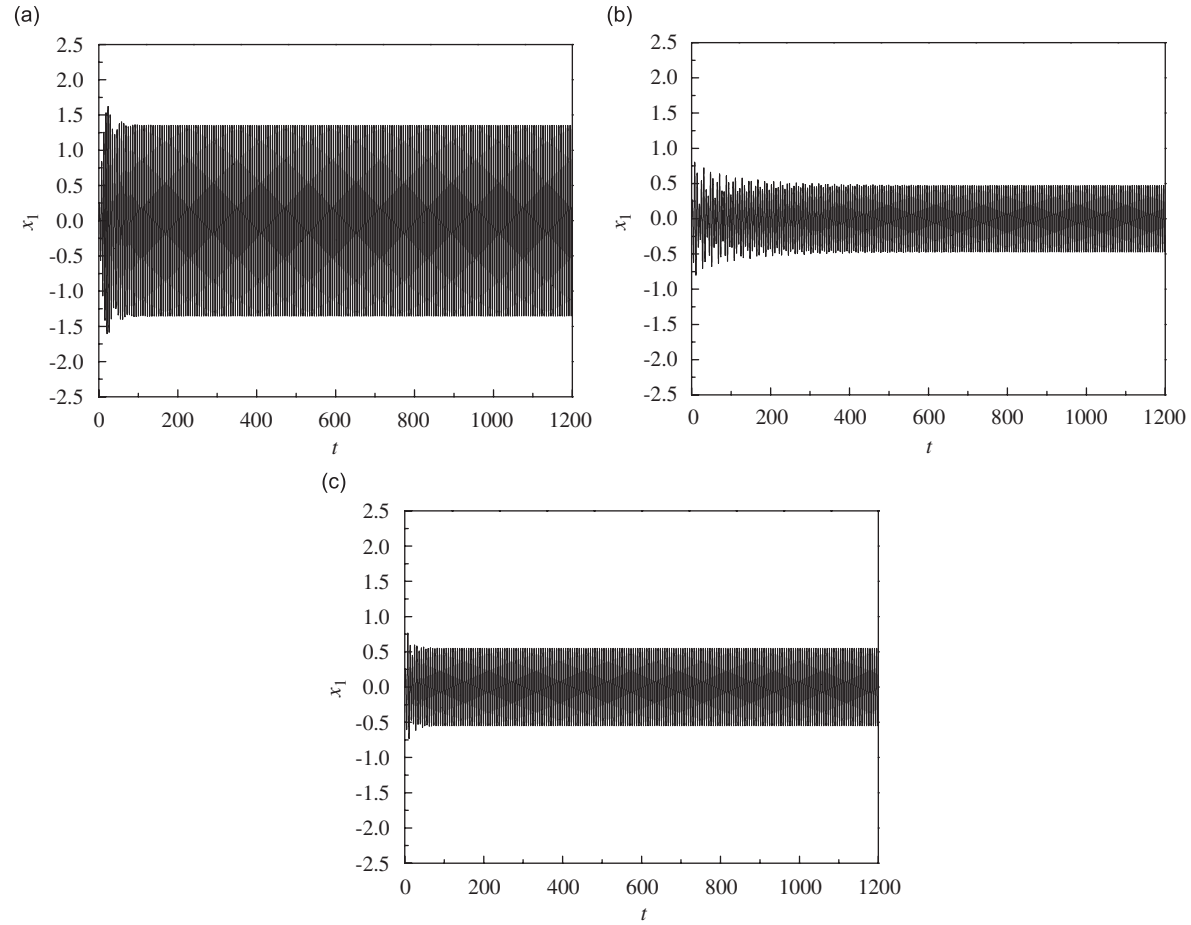

Fig. 6. Time history showing the vibration suppression when $\varepsilon g = 0.25$ for (a) $\varepsilon\tau = 0$, (b) $\varepsilon\tau = 3.0$ and (c) $\varepsilon\tau = 4.0$.

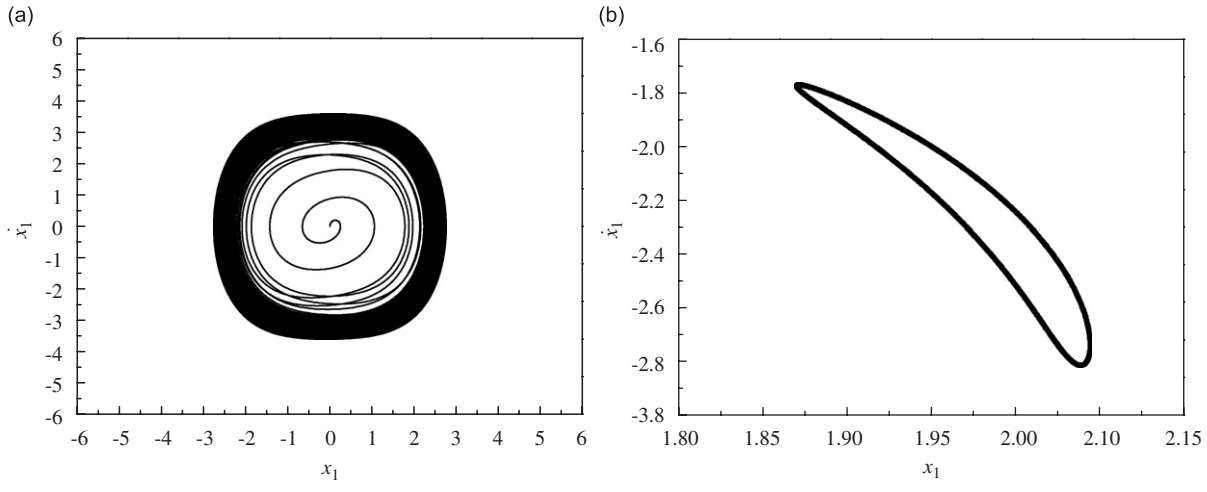

Fig. 7. Quasi-periodic motion for $\varepsilon g = 0.18$ and $\varepsilon\tau = 1.5$ (a) phase plane and (b) Poincaré section.

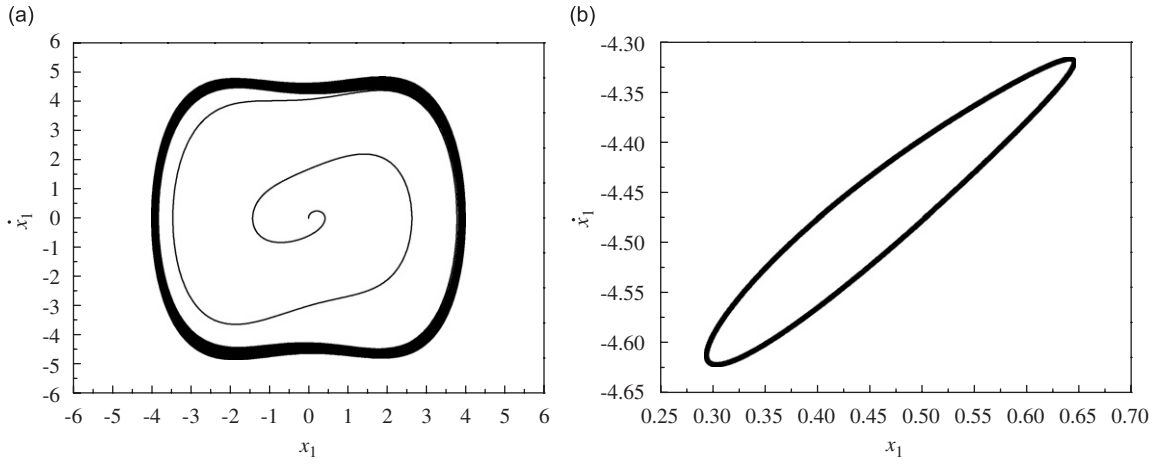

Fig. 8. Quasi-periodic motion for $\varepsilon g = 1.0$ and $\varepsilon\tau = 2.0$: (a) phase plane and (b) Poincaré section.

Finally, we observe what possible complex motions may occur by numerical method when the delay is located between H_1 and H_2. Figs. 7 and 8 show the phase plane and the Poincaré section for $\varepsilon\tau = 1.5$, $\varepsilon g = 0.18$ and $\varepsilon\tau = 2.0$, $\varepsilon g = 1.0$ (see Fig. 2g and j). The diagram in the Poincaré section is obtained by

$$\Pi = \{(x_1(t), \quad \dot{x}_1(t), \quad x_2(t), \quad \dot{x}_2(t))|x_1(t-\tau) = 0, \quad t>0\}.$$

It follows from Figs. 7 and 8 that those complex motions predicted in the analysis are all quasi-periodic since the closed curve occurs in the Poincaré section.

We have completed the numerical examination for the analytical prediction. The results show the analytical prediction is valid both quantitatively and qualitatively. This will be helpful to explain the evolution of the dynamical behavior more clearly when the delayed feedback control is adopted in the system under consideration. For example, it follows from Fig. 2d that the motion of the vertical displacement is a periodic motion as $\varepsilon\tau < 0.75$ (denoted as H_1). The solution undergoes a Hopf bifurcation at $\varepsilon\tau = 0.75$ and a quasi-periodic motion occurs in the system until $\varepsilon\tau = 2.40$(denoted as H_2). The motion returns to the periodic one for $\varepsilon\tau = 2.40$. With the delay is increased to $\varepsilon\tau = 3.40$ (denoted as SN_1), the periodic motion may jump to another stable periodic motion with a small amplitude depending on the energy level of initial condition. The multiple solutions occur in the system until $\varepsilon\tau = 4.20$ (denoted as SN_2). Then the motion returns to periodic one again. Such evolution is repeated periodically when the delay is increased further.

6. Performance of the control strategy for negative delayed feedback control

Now we consider the case of the negative feedback control with the time delay, i.e. $\varepsilon g < 0$. The amplitude–delay response curve is shown in Fig. 9 by calculating Eqs. (29)–(32), where $H_{(.)}$ are denoted as the Hopf bifurcation points, $SN_{(.)}$ the saddle–node bifurcation points. The solid line represents stable solutions, dot with black represents unstable foci and dot with blank represents other unstable solutions.

Fig. 9a shows the amplitude–delay response curves when $\varepsilon g = -0.10$. The amplitude decreases as $\varepsilon\tau$ increases at the beginning. Subsequently, the amplitude increases when $\varepsilon\tau$ is increased. It is obvious to see that the vibration of vertical displacement is suppressed for almost all values of the time delay. With εg increasing to -0.15, the solution undergoes a Hopf bifurcation at H_1 and H_2 as is shown in Fig. 2b. It indicates the complicated motions may occur when $\varepsilon\tau$ is located between H_1 and H_2. With εg is increased further, the saddle–node bifurcation occurs at SN_1 and SN_2 (see Fig. 2c). A stable and an unstable solution coexist for those values of $\varepsilon\tau$ between SN_1 and SN_2. Correspondingly, the maximum suppressed amplitude is improved by increasing the εg. However, the tunable range of $\varepsilon\tau$ for vibrations suppression shrinks.

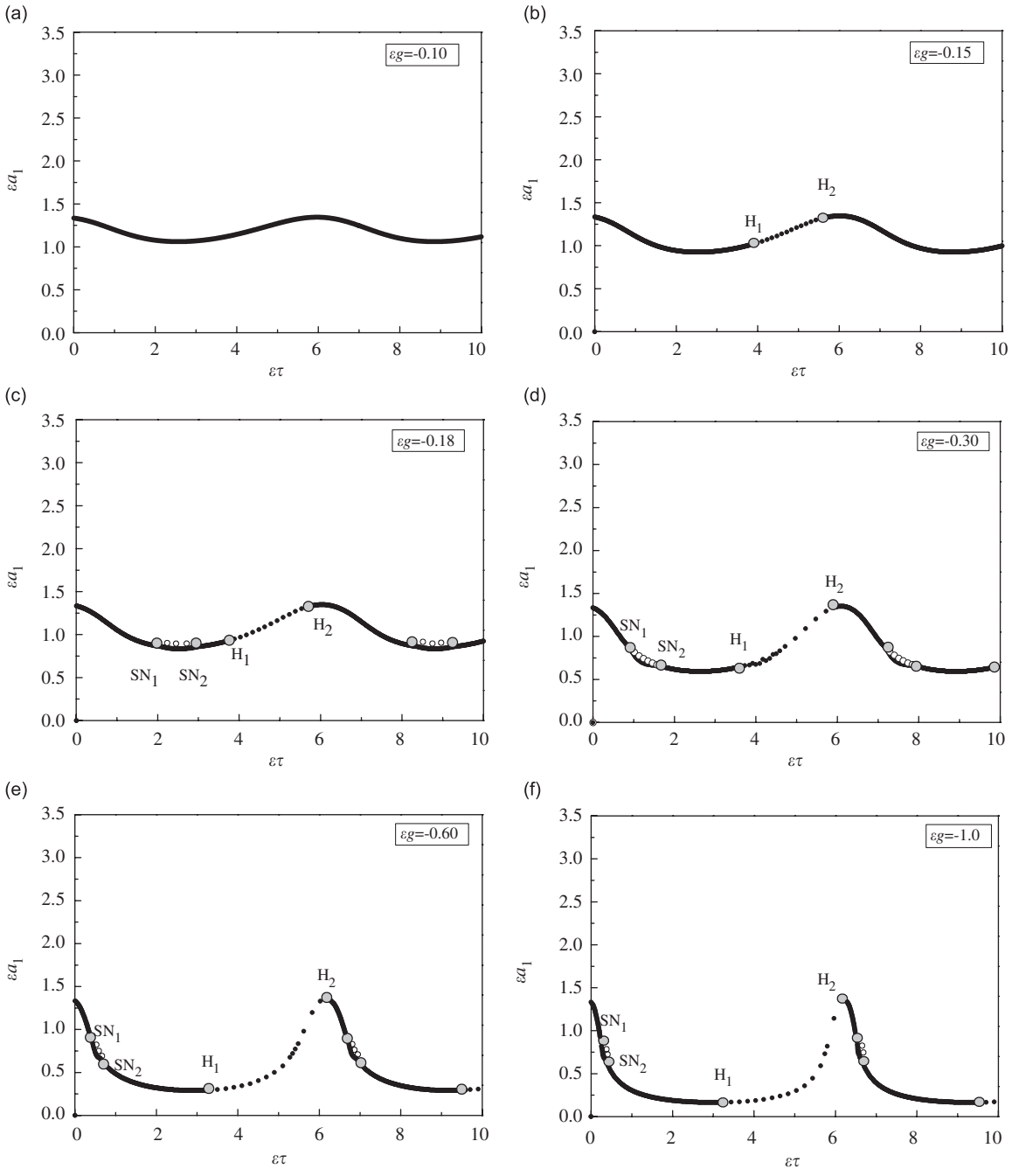

Fig. 9. Amplitude–delay response curves of vertical displacement with different gains for negative delayed feedback control.

We notice that the topological structure of the amplitude–delay response curves is the same from Fig. 9c to f. The vibration of the vertical displacement could be suppressed to a great extent and complex motions may occur simultaneously in the system under consideration by tuning the gain and the time delay.

The above analysis clearly shows that a better performance of vibration suppression is attained for the negative delayed feedback. Although a small value of the gain can provide large range of $\varepsilon\tau$ to suppress the vibration, the benefit of the suppression is not in evidence. For a large value of the gain, the effect of suppressing vibration is very clear but the tunable range of the time delay becomes narrow. In addition, a large

value of the gain may lead to the complicated motions occurring in the system for some values of the time delay between H_1 and H_2.

Now we perform a series of numerical results derived from Eqs. (3) and (4), to confirm various predictions mentioned above. The initial conditions are taken as $x_1(0) = x_2(0) = 10^{-4}$, $\dot{x}_1(0) = \dot{x}_2(0) = 10^{-4}$, $x_1(t) = x_2(t) = 0$, $\dot{x}_1(t) = \dot{x}_2(t) = 0$ for $t \in [-\varepsilon\tau, 0)$. The parameters are the same as those in Fig. 9.

First, the comparison of the results between numerical simulation and analytical solutions is shown in Fig. 10 when $\varepsilon g = -0.10$, where the solid line represents the analytical solution and the dot with asterisk symbol the numerical result. It can be seen that the numerical simulation agrees with the analytical solutions well corresponding to Fig. 9a, which suggests that the analytical predictions are valid.

It has been predicted from the above analytical solutions that the effect of suppressing vibration is very clear for a large value of the gain. We chose two cases corresponding to Fig. 9d and f (see Fig. 11) to verify the prediction quantitatively. It is obviously to see that the amplitude of the vertical displacement is maximally suppressed about 55% when $\varepsilon g = -0.30$ and about 86% when $\varepsilon g = -0.10$. The analytical solutions agree with the numerical simulations well by comparing Fig. 11 with Fig. 9.

We have predicted from the above analytical solutions that complex motions may occur when delay is located between H_1 and H_2. Correspondingly, we observe that chaotic motions occur in some values of time

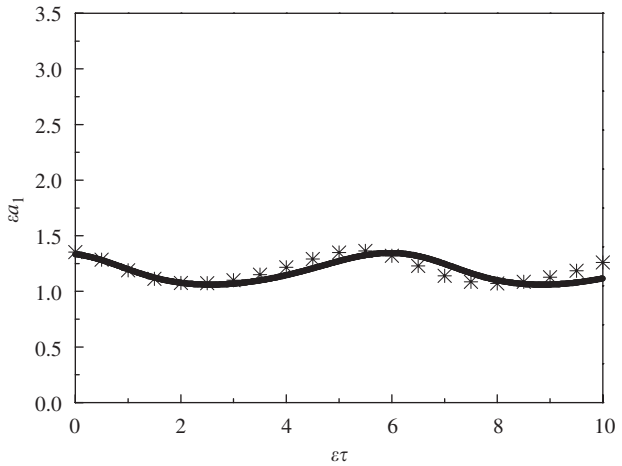

Fig. 10. Comparison between numerical simulation and analytical solution for amplitude–delay response curves when $\varepsilon g = -0.10$.

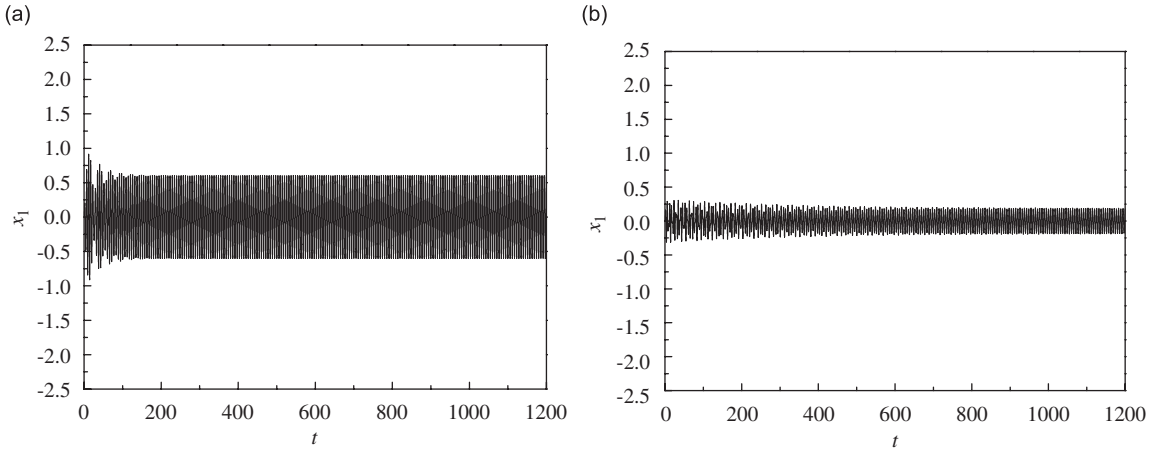

Fig. 11. Time history showing the vibration suppression (a) $\varepsilon g = -0.30$, $\varepsilon\tau = 2.5$ and (b) $\varepsilon g = -1.0$, $\varepsilon\tau = 3.0$.

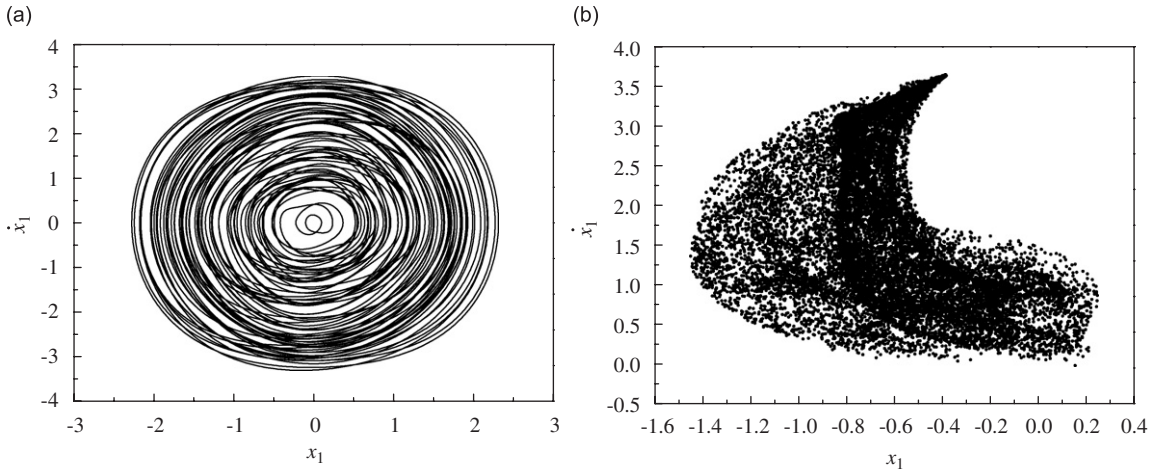

Fig. 12. Chaotic motion for $\varepsilon g = -0.60$ and $\varepsilon\tau = 4.0$: (a) phase plane and (b) Poincaré section.

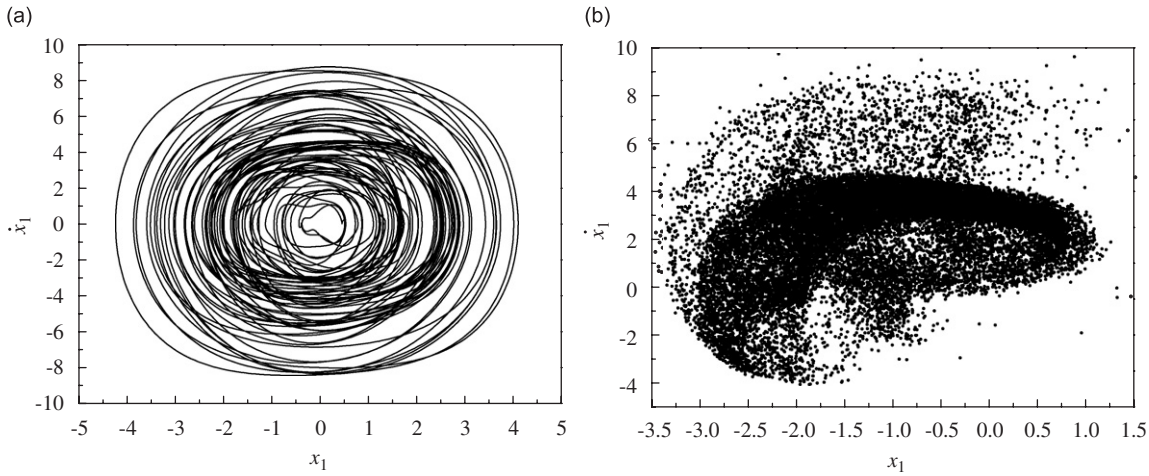

Fig. 13. Chaotic motion for $\varepsilon g = -1.0$ and $\varepsilon\tau = 5.0$: (a) phase plane and (b) Poincaré section.

delay by numerical method. Figs. 12 and 13 show the phase plane and Poincaré section for $\varepsilon g = -0.60$, $\varepsilon\tau = 4.0$ and $\varepsilon g = -1.0$, $\varepsilon\tau = 5.0$ (see Fig. 9e and f). In the following cases, the diagram in the Poincaré section is obtained by

$$\Pi = \{(x_1(t), \quad \dot{x}_1(t), \quad x_2(t), \quad \dot{x}_2(t))|x_1(t-\tau) = 0, t>0\}.$$

It follows from Figs. 12 and 13 that those complex motions predicted in the above prediction are chaotic motions as Poincaré section has the appearance of a strange attracter.

Finally, the evolution of the dynamical behavior under consideration may be illustrated by numerical method. For the case of $\varepsilon g = -0.30$, the Poincaré section for different values of τ is shown in Fig. 14. The motion of the vertical displacement is periodic when $\varepsilon\tau < 3.5$ (denoted as H_1 in Fig. 9d) as shown in Fig. 14a. The solution undergoes a bifurcation at $\varepsilon\tau = 3.5$ and a quasi-periodic motion occurs. It can be confirmed by Fig. 14b. When the delay is increased, the system enters the chaotic motions and a strange attractor occurs in the Poincaré section as shown in Fig. 14c. When $\varepsilon\tau$ is increased further, the quasi-periodic motion occurs again in the system until $\varepsilon\tau = 6.0$ (denoted as H_2 in Fig. 9d). Correspondingly, a closed curve occurs in the Poincaré section (see Fig. 14d). For the much larger values of τ, the periodic motion occurs in the system again as shown in Fig. 14e. Such evolution is also found by Xu and Yu [31].

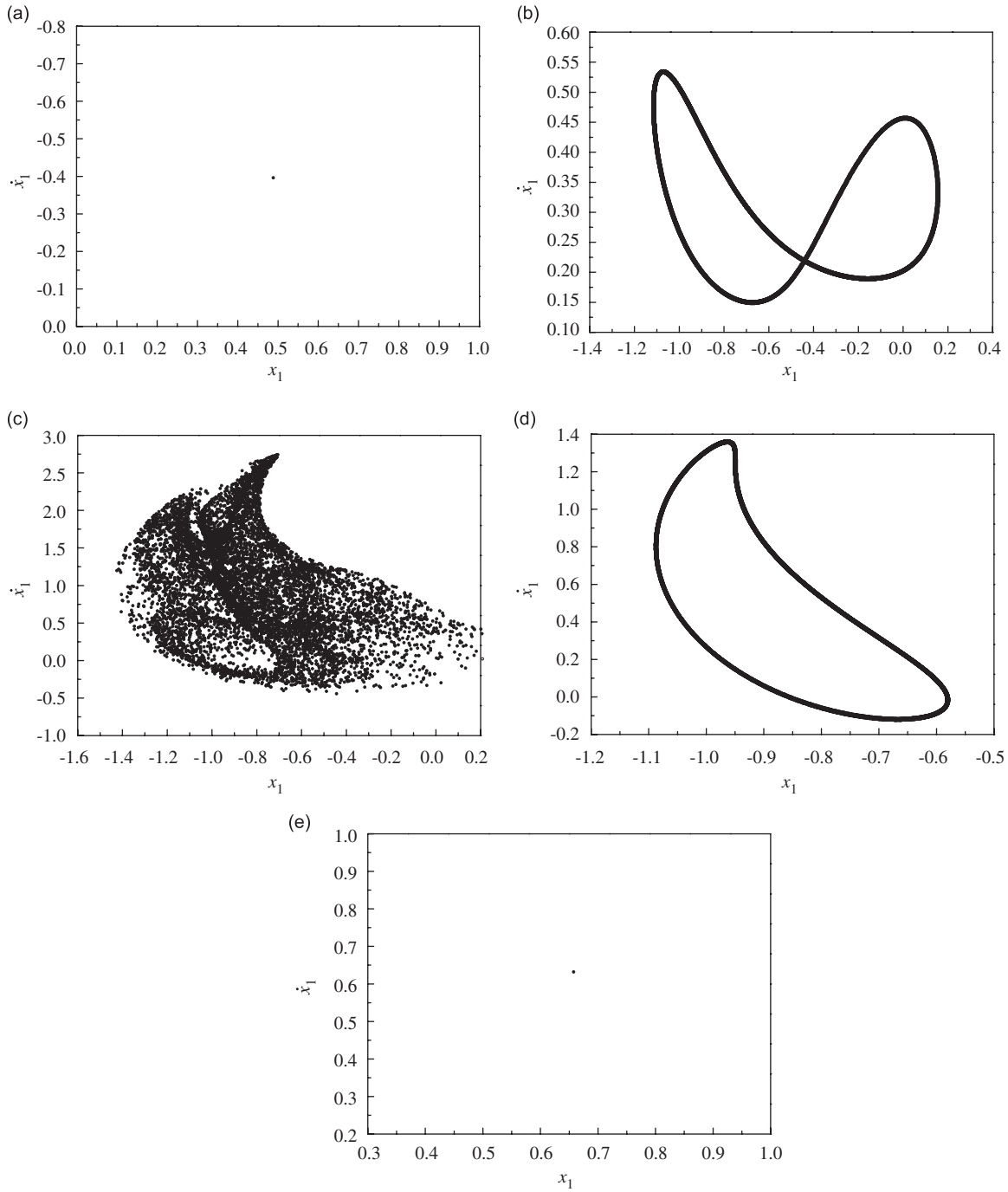

Fig. 14. Poincaré section for $\varepsilon g = -0.30$: (a) $\varepsilon\tau = 2.0$, (b) $\varepsilon\tau = 4.2$, (c) $\varepsilon\tau = 4.5$, (d) $\varepsilon\tau = 5.0$ and (e) $\varepsilon\tau = 6.5$.

Based on the analysis of Fig. 14, it is easy to see that the motion of the system undergoes the process of periodic–quasi-periodic–chaotic–quasi-periodic–periodic motions. The process just displays the routes to chaos, that is from quasi-periodic motions to chaotic ones. It follows that time delay plays an important role in the dynamic system under consideration. For a fixed gain, time delay may be used as a control parameter. It may not only be used to suppress the vibration to be controlled but also may control complex dynamical behaviors, such as quasi-periodic motions and chaotic motions.

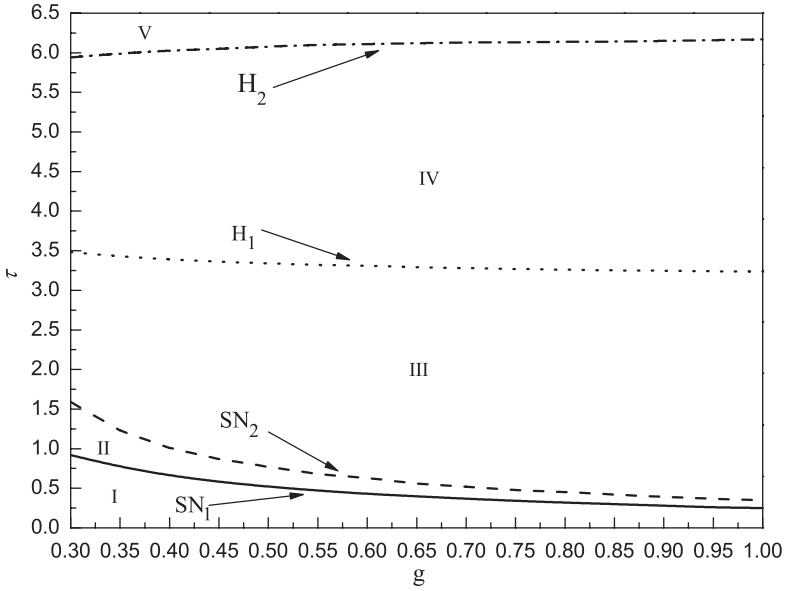

Fig. 15. Bifurcation curves for Hopf and saddle–node.

It is clear that the negative delayed feedback control can provide more range of $\varepsilon\tau$ than the positive one to suppress the vibration of the system under consideration. Moreover, the vibration of vertical displacement could be maximally suppressed about 86% for the former and 65% for the latter by comparing with the nonlinear vibration absorber without delayed feedback control. However, the negative delayed feedback control may lead to chaotic motions at some values of $\varepsilon\tau$, while the positive one may only result in quasi-periodic motions.

In order to analyze the effect of both gain and time delay on dynamical behavior for negative delayed feedback control, the bifurcation curves for Hopf and saddle–node are shown in Fig. 15.

Fig. 15 shows that the bifurcation curves divide the plane into five regions. The dynamical behaviors of the system are shown as follows in different divisions.

The system has a stable equilibrium solution in region I, III and V. The motion of the system is periodic in these regions. A stable and an unstable equilibrium solution coexist in region II. Correspondingly, jump phenomena may occur in this region. In region IV, the equilibrium solution of the system is unstable focus. Quasi-periodic or chaos motion may occur in this region.

7. Conclusion

We propose a delayed feedback control in a two-degree-of-freedom nonlinear system with external excitation. The position feedback control with time delay has been studied for the primary resonance and 1:1 internal resonance of a nonlinear vibration absorber simultaneously. We develop the governing equations and obtain the approximate solutions of the delayed differential equations by the method of multiple scales. Analytical solutions are used to analyze and understand the mechanism that makes the vibration absorber work. Moreover, the analytical predictions are in good agreement with numerical simulation both quantitatively and qualitatively. The focus is the effect of the gain and the delay on the performance of the vibration suppression since they are often used as control parameters for vibration suppression. Two control strategies for positive and negative delayed feedback have been investigated respectively.

For the case of positive delayed feedback control, a tunable range of $\varepsilon\tau$ is obtained to suppress the vibration of the system under consideration. The vibration of vertical displacement is maximally suppressed about 65% by comparing with the nonlinear vibration absorber without delayed feedback control. Yet, at some values of time delay that the vibration suppression is invalid, complex motions may occur in the system. For the case of negative delayed feedback control, a tunable range of $\varepsilon\tau$ is also obtained to suppress the vibration of

the system. Moreover, the vibration of vertical displacement is maximally suppressed about 86% by comparing with the nonlinear vibration absorber without delayed feedback control. But the chaotic motions may occur at some values of time delay.

We have noticed that, for positive and negative delayed feedback control strategies, the maximum vibration suppression point is improved for a large value of the gain. But it may lead to the system losing stability such that the motion becomes complicated. Therefore, the gain should be modified very carefully in applications. We remark that for a fixed gain, time delay plays an important role in the dynamical system. It may be used as a control parameter not only to suppress the vibration but also to generate complex motions in the dynamical system, such as quasi-periodic motions and chaotic motions.

Acknowledgments

This research is supported by the NNSF of China under Grant No. 10532050 and the National Outstanding Young Funds of China under Grant No. 10625211.

References

[1] W.J. Ding, *Theory of Vibration Absorption*, Tsinghua university, Beijing, 1988.
[2] R. Roberson, Synthesis of a nonlinear dynamical vibration absorber, *Journal of the Franklin Institute* 254 (1952) 205–220.
[3] F. Arnold, Steady-state behavior of systems provide with nonlinear dynamic vibration absorbers, *Journal of Applied Mechanics* 22 (1995) 487–492.
[4] C. Lee, S. Shaw, The non-linear dynamic response of paired centrifugal pendulum vibration absorbers, *Journal of Sound and Vibration* 203 (5) (1997) 731–743.
[5] A. Nayfeh, D. Mook, L. Marshall, Nonlinear coupling of pitch and roll in ship motion, *Journal of Hydronautics* 7 (4) (1973) 145–152.
[6] S. Oueini, M.F. Golnaraghi, Experimental implementation of the internal resonance control strategy, *Journal of Sound and Vibration* 191 (3) (1996) 377–396.
[7] S. Oueini, A. Nayfeh, Analysis and application of a nonlinear vibration absorber, *Journal of Vibration and Control* 6 (7) (2000) 999–1016.
[8] P. Pai, B. Wen, A. Naser, M. Schultz, Structural vibration control using PZT patches and non-linear phenomena, *Journal of Sound and Vibration* 215 (1998) 273–296.
[9] J. Pratt, S. Oueini, A. Nayfeh, A Terfenol-D nonlinear vibration absorber, *Journal of Intelligent Material Systems and Structures* 10 (1999) 29–35.
[10] S.Y. Chu, T.T. Soong, C.C. Lin, Y.Z. Chen, Time-delay effect and compensation on direct output feedback controlled mass damper system, *Earthquake Engineering and Structural Dynamics* 32 (2002) 121–137.
[11] M.S. Fofana, Sufficient conditions for the stability of single and multiple regenerative chatter, *Chaos, Solitons and Fractals* 14 (2002) 335–347.
[12] A.M. Gouskov, S.A. Voronov, H. Paris, S.A. Batzer, Nonlinear dynamics of a machining system with two interdependent delays, *Communications in Nonlinear Science and Numerical Simulation* 7 (2002) 207–221.
[13] M.S. Fofana, Delay dynamical systems and applications to nonlinear machine-tool chatter, *Chaos, Solitons and Fractals* 17 (2003) 731–747.
[14] E. Zervas, Comparative study of some experimental methods to characterize the combustion in a SI engine, *Energy* 30 (2005) 1803–1816.
[15] L. Librescu, P. Marzocca, W.A. Silva, Aeroelasticity of 2-D lifting surfaces with time-delayed feedback control, *Journal of Fluids and Structures* 20 (2005) 197–215.
[16] C. Li, X.F. Liao, K.W. Wong, Chaotic lag synchronization of coupled time-delayed systems and its applications in secure communication, *Physica D* 194 (2004) 187–202.
[17] L. Geng, K. Osusky, S. Konjeti, A. Fu, D. Hallahan, Radiation-guided drug delivery to tumor blood vessels results in improved tumor growth delay, *Journal of Controlled Release* 99 (2004) 369–381.
[18] S. Ellen, T. Fejel, R.F. Pommier, Relationships among delay of diagnosis, extent of disease, and survival in patients with abdominal carcinoid tumors, *The American Journal of Surgery* 187 (2004) 575–579.
[19] K. Pyragas, Continuous control of chaos by self-controlling feedback, *Physics Letter A* 170 (1992) 421–428.
[20] J. Xu, K.W. Chung, Effects of time delayed position feedback on a van der Pol-Duffing oscillator, *Physica D* 180 (1) (2003) 17–39.
[21] N. OLgac, B.T. Holm-Hansen, A novel active vibration absorption technique: delayed resonator, *Journal of Sound and Vibration* 176 (1) (1996) 93–104.
[22] N. Jalili, N. Olgac, Multiple delayed resonator vibration absorbers for multi-degree-of-freedom mechanical structures, *Journal of Sound and Vibration* 223 (4) (1999) 567–585.
[23] N. Olgac, M. Hosek, A new perspective and analysis for regenerative machine tool chatter, *International Journal of Machine Tool and Manufacture* 38 (1998) 783–798.

[24] D. Filipovic, N. Olgac, Delayed resonator with speed feedback-design and performance analysis, *Mechatronics* 12 (2002) 393–413.
[25] N. Olgac, R. Sipahi, An exact method for the stability analysis of time-delayed linear time-invariant (LTI) system, *IEEE Transactions on Automatic Control* 47 (5) (2002) 793–797.
[26] S.T. Ariaratnam, Random vibrations of nonlinear suspensions, *Journal of Mechanical Engineering Sciences* 2 (1960) 195–201.
[27] N. Malhotra, N. Srinamachchivaya, Global bifurcations in externally excited two-degree-of-freedom nonlinear systems, *Nonlinear Dynamics* 8 (1995) 85–109.
[28] W. Zhang, J. Li, Global analysis for a nonlinear vibration absorber with fast and slow modes, *International Journal of Bifurcation and Chaos* 8 (2001) 2179–2194.
[29] A. Nayfeh, D. Mook, *Nonlinear Oscillations*, Wiley, New York, 1979.
[30] S. Wirkus, R. Rand, The dynamics of two coupled van der Pol oscillators with delay coupling, *Nonlinear Dynamics* 30 (2002) 205–221.
[31] J. Xu, P. Yu, Delay-induced bifurcations in a nonautonomous system with delayed velocity feedbacks, *International Journal of Bifurcation and Chaos* 14 (8) (2004) 2777–2798.